Quantifying vegetation indices using Terrestrial Laser Scanning: methodological complexities and ecological insights from a Mediterranean forest

William Rupert Moore Flynn[1], Harry Jon Foord Owen[2], Stuart William David Grieve[1,3] and Emily Rebecca Lines[2]

[1]School of Geography, Queen Mary University of London, Mile End Rd, Bethnal Green, London E1 4NS

[2]Department of Geography, University of Cambridge, Downing Place, Cambridge, CB2 3EN

[3]Digital Environment Research Institute, Queen Mary University of London, New Road, London, E1 1HH

Correspondence to: W. R. M. Flynn (w.r.m.flynn@qmul.ac.uk)

Abstract. Accurate measurement of vegetation density metrics including plant, wood and leaf area indices (PAI, WAI and LAI) is key to monitoring and modelling carbon storage and uptake in forests. Traditional passive sensor approaches, such as Digital Hemispherical Photography (DHP), cannot separate leaf and wood material, nor individual trees, and require many assumptions in processing. Terrestrial Laser Scanning (TLS) data offer new opportunities to improve understanding of tree and canopy structure. Multiple methods have been developed to derive PAI and LAI from TLS data, but there is little consensus on the best approach, nor are methods benchmarked as standard.

Using TLS data collected in 33 plots containing 2472 trees of five species in Mediterranean forests, we compare three TLS methods (*LiDAR Pulse*, *2D Intensity Image* and *Voxel-Based*) to derive PAI and compare with co-located DHP. We then separate leaf and wood in individual tree point clouds to calculate the ratio of wood to total plant area (α), a metric to correct for non-photosynthetic material in LAI estimates. We use individual tree TLS point clouds to estimate how α varies with species, tree height and stand density.

We find the *LiDAR Pulse* method agrees most closely with DHP, but is limited to single scan data so cannot determine individual tree properties, including α. The *Voxel-Based* method shows promise for ecological studies as it can be applied to individual tree point clouds. Using the *Voxel-Based* method, we show that species explain some variation in α, however, height and plot density were better predictors.

Our findings highlight the value of TLS data to improve fundamental understanding of tree form and function, but also the importance of rigorous testing of TLS data processing methods at a time when new approaches are being rapidly developed. New algorithms need to be compared against traditional methods, and existing algorithms, using common reference data. Whilst promising, our results show that metrics derived from TLS data are not yet reliably calibrated and validated to the extent they are ready to replace traditional approaches for large scale monitoring of PAI and LAI.

1 Introduction

Leaf Area Index (LAI), defined as half the amount of green leaf area per unit ground area (Chen and Black, 1992), determines global evapotranspiration, phenological patterns and canopy photosynthesis, and is therefore an essential climate variable (ECV), as well as a key input in dynamic global vegetation models (Sea et al., 2011; Weiss et al., 2004). Accurate measurements of leaf, wood and plant area indices (LAI, WAI and PAI) have historically been derived from labour intensive destructive sampling (Baret et al., 2013; Jonckheere et al., 2004), so over large spatial or temporal scales these can only be measured indirectly, typically with remote sensing. Large-scale remote sensing, using spaceborne and airborne instruments, has been widely used to estimate LAI over large areas (Pfeifer et al., 2012), but requires calibration and validation using in situ measurements to constrain information retrieval (Calders et al., 2018). Non-destructive in situ vegetation index estimates have historically been made by measuring light transmission below the canopy and using simplifying assumptions about canopy structure to estimate the amount of intercepting material (e.g. Beer-Lambert's law; Monsi and Saeki, 1953). The most common method, Digital Hemispherical Photography (DHP; Figure 1a), requires both model assumptions and subjective user choices during data acquisition and processing in order to estimate both PAI and LAI (Breda, 2003). DHP images are processed by separating sky from canopy, but not photosynthetic from non-photosynthetic vegetative material, so additional assumptions are needed to calculate either LAI or WAI (Jonckheere et al., 2004; Pfeifer et al., 2012). Separation of LAI from PAI can be achieved by removing or masking branches and stems from hemispherical images (e.g. Sea et al., 2011; Woodgate et al., 2016), but is not reliable when leaves are occluded by woody components (Hardwick et al., 2015). An alternative approach is to take separate DHP measurements in both leaf on and leaf off conditions, and derive empirical wood to plant ratios (WAI/PAI, α) (Leblanc and Chen, 2001), but this is not always practical, for example in evergreen forests. The difficulty of separation means that studies often omit correcting for the effect of WAI on optical PAI measurements altogether (Woodgate et al., 2016), but since woody components in the forest canopy can account for more than 30% of PAI (Ma et al., 2016) this can introduce overestimation. Further, although DHP estimates of LAI or PAI are valuable both for ecosystem monitoring and developing satellite LAI products (Hardwick et al., 2015; Pfeifer et al., 2012), they are limited to sampling only at a neighbourhood or plot level (Weiss et al., 2004), and cannot be used to measure individual tree LAI except for open grown trees (Béland et al., 2014).

The ratio of wood to total plant area, α, is known to be dynamic, changing in response to abiotic and biotic conditions. For example, the Huber value (sapwood to leaf area ratio, a related measure to α) may vary according to water availability (Carter and White, 2009). Leaf area may therefore be indicative of the drought tolerance level of a tree, with more drought tolerant species displaying a lower leaf area, reducing the hydraulic conductance of the whole tree and therefore increasing its drought tolerance (Niinemets and Valladares, 2006). α has been hypothesised to increase with the size of a tree in response to the increased hydraulic demand associated with greater hydraulic resistance of tall trees (Magnani et al., 2000) and higher transpiration rates of larger LAI (Battaglia et al., 1998; Phillips et al., 2003). Stand density may also impact α (Long and Smith, 1988; Whitehead, 1978), as increased stand level water use scales linearly with LAI (Battaglia et al., 1998; Specht and Specht, 1989), reducing water availability to individual trees competing for the same resources (Jump et al., 2017). Large scale quantification of α or Huber value, however, is difficult as studies usually rely on a small number of destructively sampled trees (e.g. Carter and White, 2009; Magnani et al., 2000), litterfall traps (e.g. Phillips et al., 2003) or

72　masking hemispherical images (e.g. Sea et al., 2011; Woodgate et al., 2016). These approaches are only applicable

73　on a small to medium scale, and in the case of image masking, cannot differentiate between individuals. Variation

74　in α, for example by species and or stand structure, is therefore largely unknown.

1.1 TLS methods for calculating PAI, LAI and WAI

76　Terrestrial Laser Scanning (TLS) generates high-resolution 3D measurements of whole forests and individual

77　trees (Burt et al., 2018; Disney, 2018), leading to the development of completely new monitoring approaches to

78　understand the structure and function of ecosystems (Lines et al., 2022). Unlike traditional passive sensors, TLS

79　can estimate PAI, WAI, and LAI for both whole plots and individual tree point clouds (Calders et al., 2018), and

80　is unaffected by illumination conditions. This has led to the development of several methods for processing TLS

81　data to extract the key metrics PAI, WAI and LAI (e.g. Hosoi and Omasa, 2006; Jupp et al., 2008; Zheng et al.,

82　2013). However, intercomparison studies of algorithms and processing approaches to derive the same metrics

83　from different TLS methods are lacking.TLS methods for extracting PAI, LAI and WAI can be broadly

84　categorised into two types: (1) LiDAR return counting, using single scan data (e.g., the *LiDAR Pulse* method;

85　Jupp et al., 2008, and *2D Intensity Image* method; Zheng et al., 2013) and (2) point cloud voxelisation, usually

86　using co-registered scans (e.g., the *Voxel-Based* method; Hosoi and Omasa, 2006).

87　The *LiDAR Pulse* method (Jupp et al., 2008; Figure 1b) estimates gap fraction (P_{gap}) using single scan data, as a

88　function of the total number of outgoing LiDAR pulses from the sensor and the number of pulses that are

89　intercepted by the canopy. This method, which eliminates illumination impacts associated with the use of DHP

90　(Calders et al., 2014), has been implemented in the python module, *PyLidar* (www.pylidar.org) and the R package,

91　*rTLS* (Guzman, et al. 2021). Using the *LiDAR Pulse* method, Calders et al. (2018) compared PAI estimates from

92　two ground-based passive sensors (LiCOR LAI-2000 and DHP) with TLS data collected with a RIEGL VZ-400

93　TLS in a deciduous woodland, and found the two passive sensors underestimated PAI values compared to TLS,

94　with differences dependent on DHP processing and leaf on/off conditions.

95　The *2D Intensity Image* method (Zheng et al., 2013; Figure 1c)*,* also uses raw single scan TLS point clouds, but,

96　unlike the *LiDAR Pulse* method, converts LiDAR returns into 2D panoramas where pixel values represent return

97　intensity. PAI is estimated by classifying pixels as sky or vegetation, based on their intensity value, to estimate

98　P_{gap}, and then applying Beer-Lambert's law. Like the *LiDAR Pulse* method, this approach has been shown to

99　generate higher PAI estimates than DHP (Calders et al., 2018; Woodgate et al., 2015; Grotti et al., 2020), with

100　differences attributed to the greater pixel resolution and viewing distance of TLS resolving more small canopy

101　details (Grotti et al., 2020).

102　The *Voxel-Based* method (Figure 1d) estimates PAI by segmenting a point cloud into voxels and either simulating

103　radiative transfer within each cube (Béland et al., 2014; Kamoske et al., 2019), or classifying voxels as either

104　containing vegetation or not, and dividing vegetation voxels by the total number of voxels (Hosoi and Omasa,

105　2006; Itakura and Hosoi, 2019; Li et al., 2017). Crucially, this method may be applied to multiple co-registered

106　scan point clouds and so can be used to calculate PAI for both whole plots and individual, segmented TLS trees.

107　However, PAI estimates derived using the voxel method are highly dependent on voxel size (Calders et al., 2020).

108　Using a radiative transfer approach, Béland et al. (2014) demonstrated that voxel size is dependent on canopy

109　clumping, radiative transfer model assumptions and occlusion effects*,* making a single, fixed choice of voxel size

110   for all ecosystem types, scanners or datasets impossible. To test various approaches to selecting voxel size using

111   a voxel classification approach, Li et al. (2016) matched voxel size to point cloud resolution, individual tree leaf

112   size, and minimum beam distance and tested against destructive samples, finding that voxel size matched to point

113   cloud resolution had the closest PAI values to destructive samples. The *LiDAR Pulse* method and *2D Intensity*

114   *Image* method both use single scan data. However, to generate robust estimates of canopy properties that avoid

115   errors from occlusion effects, multiple co-registered scans taken from different locations are likely needed (Wilkes

116   et al., 2017). Further, both these methods require raw unfiltered data to accurately measure the ratio of pulses

117   emitted from the scanner and number of pulses that are intercepted by vegetation. This means "noisy" points
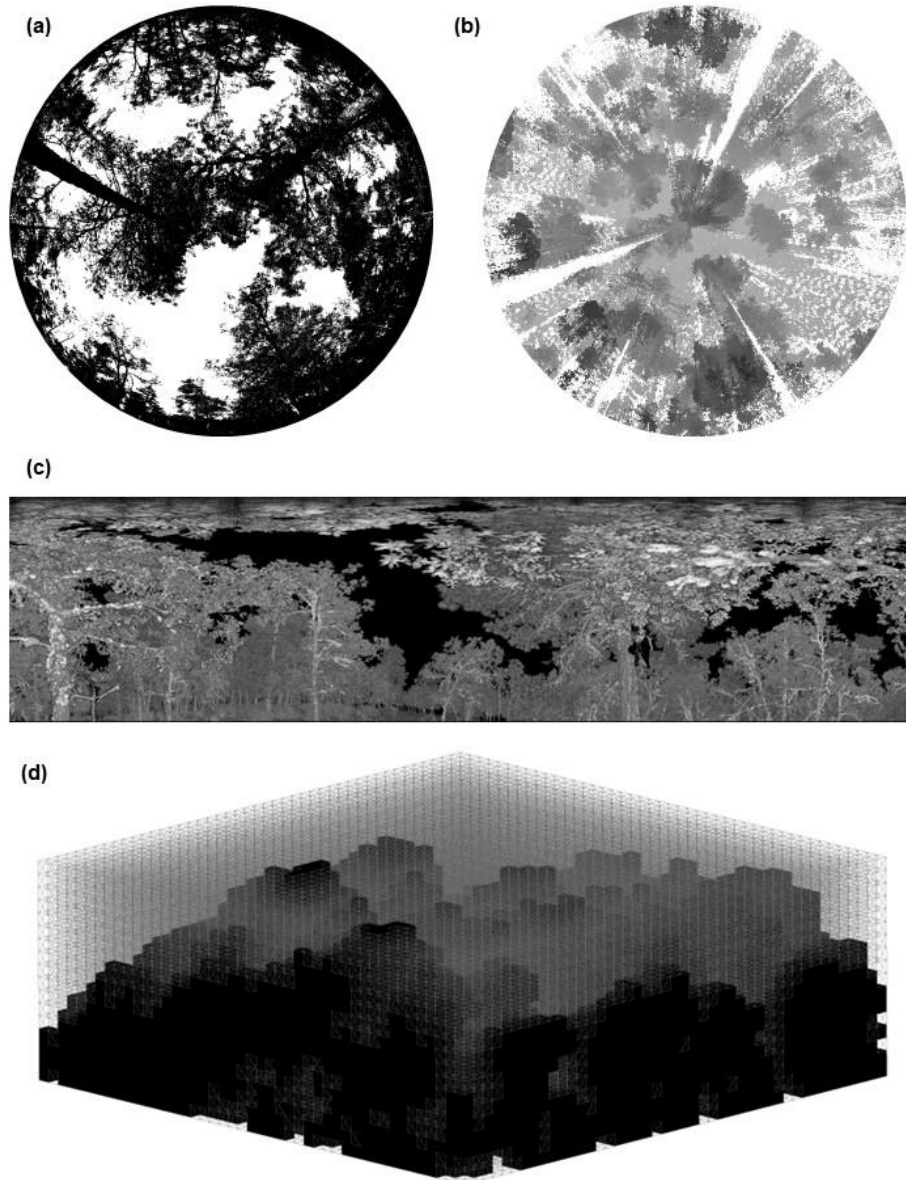
118   caused by backscattered pulses (Wilkes et al., 2017) are included in analyses, potentially leading to higher PAI

119   estimates. However, the *LiDAR Pulse* and *2D Intensity Image* methods may introduce fewer estimation errors

120   compared to DHP, which is influenced by differences in sky illumination conditions and camera exposure (Weiss

121   et al., 2004).

122

123

Figure 1: Visual representation of the four methods for PAI and WAI estimation used in this study: (a) a binarised digital hemispherical photograph (DHP), (b) TLS raw single scan point cloud, for the *LiDAR Pulse* method (Jupp et al., 2008). Image shows a top-down view of raw point cloud and greyscale represents low (grey) and high (black) Z values, (c) TLS 2D intensity image for the *2D Intensity Image* method (Zheng et al., 2013), (d) Voxelised co-registered whole plot point cloud for the *Voxel-Based* method (Hosoi and Omasa, 2006), showing a representative schematic of cube voxels with edge length of 1m, voxelised using the *R package VoxR* (Lecigne et al., 2018). Solid black voxels are classified as containing vegetation (filled) and voxels outlined with grey lines are voxels classified as empty.

1.2 Scope and aims

The aims of this study are twofold: the first aim is to compare three TLS methods for estimating PAI with traditional DHP. The second aim of this study is to use TLS to understand drivers of individual tree α variation.

In this study we use a dataset of 528 co-located DHP and high-resolution TLS scans from 33 forest plots to compare DHP derived PAI (PAI_{DHP}) with estimates from three methods to estimate PAI from TLS data (PAI_{TLS}): the *LiDAR Pulse* method; the *2D Intensity Image* method and the *Voxel-Based* method (Figure 1). We use a dataset collected from a network of pine/oak forest plots in Spain (Owen et al., 2021) and ask **(1)** are the three TLS methods able to reproduce PAI_{DHP} estimates at single scan and whole plot level? **(2)** does α, calculated from the *Voxel-Based* method on individual tree point clouds, vary with species and tolerance to drought? and **(3)** does α scale with height and stand density?

2. Methods

2.1 Study site

We collected TLS and DHP data from 29 plots in Alto Tajo Natural Park (40°41′N, 02°03′W; FunDIV – Functional Diversity plots; see Baeten et al. (2013) for a detailed description of the plots) and four plots in Cuellar (41°23′N 4°21′W) in June - July 2018 (see Owen et al. (2021) for full details) (Figure A1). Plots contained two oak species: semi-deciduous *Q. faginea* and evergreen *Q. ilex,* and three pine species: *P. nigra, P. pinaster* and *P. sylvestris*. *P. sylvestris* is the least drought tolerant species, followed by *P. nigra, Q. faginea*, *Q. ilex*; shade tolerance follows the same ranking (Niinemets and Valladares, 2006; Owen et al., 2021). Although not quantitatively ranked, *P. pinaster* has been shown to be very drought tolerant, appearing in drier areas than the other species (Madrigal-González et al., 2017). The area is characterised by a Mediterranean climate (altitudinal range 840 – 1400 m.a.s.l.) (Jucker et al., 2014; Madrigal-González et al., 2017). In addition to the five main canopy tree species, plots contained an understory of *Juniperus thurifera* and *Buxus sempervirens* (Kuusk et al., 2018).

2.2 Field protocol

In each of the 33 plots of size 30 x 30 m, we collected TLS scans on a 10 m grid, making 16 scan locations following Wilkes et al. (2017) to minimise occlusion effects associated with insufficient scans. We used a Leica HDS6200 TLS set to super high resolution (3.1 x 3.1mm resolution at 10 m with a beam divergence of $\leq$ 5 mm at 50 m; scan time 6m 44 s; see Owen et al. (2021)). At each of the 528 scan locations and following the protocol in Pfeifer et al. (2012), we captured co-located DHP images with three exposure settings (automatic and $\pm$ one stop exposure compensation), levelling a Canon EOS 6D full frame DSLR sensor with a Sigma EX DG F3.5 fisheye lens, mounted on a Vanguard Alta Pro 263AT tripod.

2.3 Calculation of single scan and whole plot PAI using DHP data

For each of the red-green-blue (RGB) DHP images we extracted the blue band for image thresholding, as this best represents sky/vegetation contrast (Pfeifer et al., 2012). For each plot, we picked the exposure setting that best represented sky/ vegetation difference based on pixel brightness histograms of four sample locations indicative of the plot. We carried out automatic image thresholding using the Ridler and Calvard method (1978), to create a binary image of sky and vegetation, avoiding subjective user pixel classification (Jonckheere et al., 2005). We calculated PAI from the binary image, limiting the field of view to a 5° band centred on the hinge angle of 57.5° (55° – 60°). The hinge angle has a path length through the canopy twice the canopy height, so the band around it is an area of significant spatial averaging taken as representative of canopy structure of the area (Calders et al., 2018; Jupp et al., 2008). From the binarised hinge angle band we calculated P_{gap} as the number of sky pixels divided by the total number of pixels and PAI using an inverse Beer-Lambert law equation (Monsi and Saeki, 1953). We calculated whole plot PAI as the arithmetic mean of the 16 plot scan location PAI estimates. As this value does not correct for canopy clumping, it is better described as effective PAI, rather than true PAI (Woodgate et al., 2015). However, as the TLS and DHP methods we apply here account for canopy clumping differently, we compared effective values and here-on refer to effective PAI as PAI (Calders et al., 2018). DHP images used in this study are freely available (see Flynn et al., 2023).

2.4 Calculation of single scan and whole plot PAI from TLS data

To calculate PAI using the *LiDAR Pulse* method (Jupp et al., 2008), we calculated P_{gap} for a single scan (Figure 1b) by summing all returned laser pulses and dividing by the number of total outgoing pulses, following Lovell et al. (2011; see Eq. 7 in that study), and then estimated PAI following Jupp et al. (2008; see Eq. 18 in that study), setting the sensor range to 5° around the hinge angle as before (55° – 60°). Single scan PAI was taken as the cumulative sum of PAI values estimated by vertically dividing the hinge region into 0.25 m intervals (Calders et al., 2014). We implemented the *LiDAR Pulse* method using the open-source *R* (R Core Team, 2020) package, *rTLS* (Guzmán and Hernandez, 2021).

To calculate PAI using the *2D Intensity Image* method (Zheng et al., 2013), we converted 3D TLS point cloud data from all 528 scan locations into polar coordinates, scaled intensity values to cover the full 0-255 range (Figure 1c) and rasterised into a 2D intensity image using the open-source *R* package, *raster* (Hijmans, 2022). We cut the 2D intensity image to a 5° band around the hinge angle (55° – 60°) and classified sky and vegetation pixels in each image using the Ridler and Calvard method (1978). We calculated P_{gap} as the number of pixels classified as sky divided by the total number of pixels and derived PAI with an inverse Beer-Lambert law equation (Monsi and Saeki, 1953).

Following the same approach as applied to our DHP data, we calculated whole plot PAI for the *LiDAR Pulse* and *2D Intensity Image* methods as the arithmetic mean of the 16 plot scan location PAI estimates.

To calculate PAI using the *Voxel-Based* method, we followed a voxel classification approach (Hosoi and Omasa, 2006), downsampling the point cloud to 0.05 m to aid computation time and matching the voxel size to the resolution of the point cloud, following Li et al. (2016), who showed that matching the voxel size to the point cloud point to point minimum distance (resolution) increases accuracy as small canopy gaps are not included in voxels classified as vegetation. We chose to use a voxel classification approach (rather than a radiative transfer

based one) as this method is widely applicable to a range of TLS systems and levels of processing, as well as providing explicit guidance on voxel size selection, which is known to impact derived PAI estimates (Li et al., 2016). We re-combined individually segmented trees, filtered for noise using a height-dependent statistical filter (see Owen et al., 2021) back into whole plot point clouds and voxelised them using the open source *R* package, *VoxR* (Lecigne et al., 2018), with a full grid covering the minimum to maximum XYZ ranges of the plot. We classified any voxel containing > 0 points as vegetation ("filled"), and empty voxels as gaps. We then split the voxelised point cloud vertically into slices one voxel high. Within each slice, the contact frequency is calculated as the fraction of filled to total number of voxels. We then multiplied the contact frequency by a correction factor for leaf inclination, set at 1.1 (Li et al., 2017), and whole plot PAI was calculated as the sum of all slices' contact frequencies.

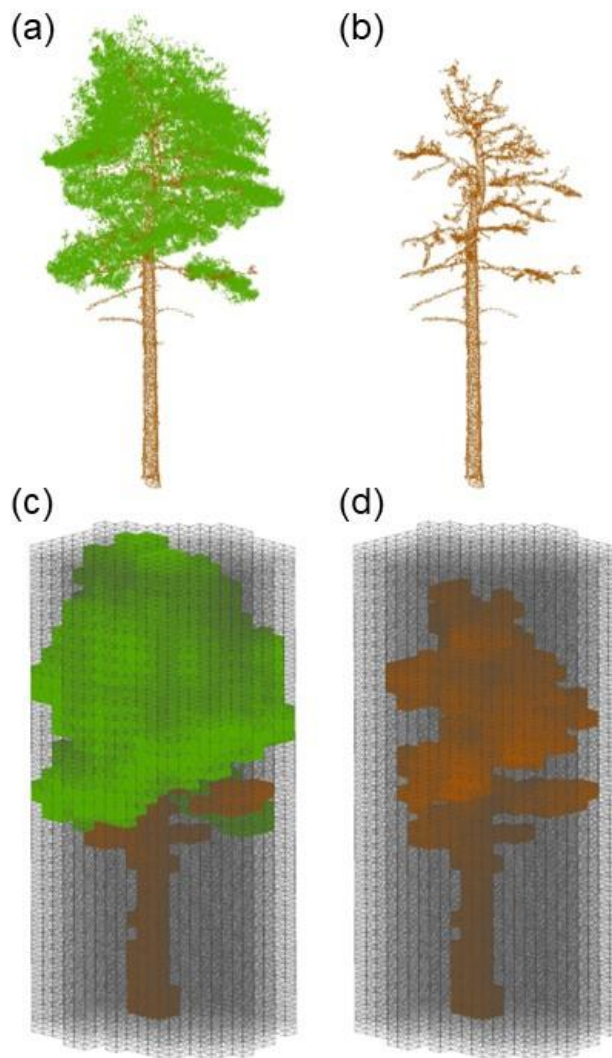**2.5 Calculation of individual tree PAI, WAI and α using the voxel-based method**

Figure 2: Visualisation of the workflow for applying the Voxel-Based method to estimate individual-tree PAI, WAI and α. (a) Individual tree point cloud; (b) separated leaf off (wood) individual tree point cloud; (c) voxelised individual tree point cloud; (d) voxelised wood cloud. Coloured voxels (green represents leaf and brown represents wood) are filled voxels and grey lines are empty voxels. Empty voxels occupy the space within the projected crown area of the tree. Image shows schematic of point cloud voxelised with cube voxels with edge length of 0.5 m. Panels (a) and (b) show wood and leaf separation of an example *P. sylvestris*, carried out using *TLSeparation* (Vicari et al., 2019). Point cloud

216 **voxelisation was carried out using modified functions from *R* package *VoxR* (Lecigne et al., 2018). Note that our method**
217 **used voxel sizes at the resolution of the cloud (0.05 m), but here we present an image with larger voxels to ease visual**
218 **interpretation.**

219 As the only method using multiple co-registered scans, the *Voxel-Based* method is only method compared in this

220 study capable of deriving PAI, WAI and LAI of segmented individual tree point clouds. We estimated PAI and

221 WAI for 2472 individual trees segmented from co-registered point clouds following a similar method to the whole

222 plot point cloud. We used individual tree point clouds downsampled to 0.05 m, to aid computation time, and

223 segmented using the automated tree segmentation program *treeseg* (Burt et al., 2019), implemented in C++, by

224 Owen et al. (2021) for that study. Individual segmented tree data used in this study are freely available (see Owen

225 et al., 2022).

226 To estimate PAI, WAI and α for each tree, we used individual tree point clouds wood – leaf separated by Owen

227 et al. (2021) using the open source Python library *TLSeparation* (Vicari et al., 2019), and then used the separated

228 wood point clouds to calculate WAI. *TLSeparation* assigns points as either leaf or wood, iteratively looking at a

229 predetermined number of nearest neighbours (*knn*). The *knn* of each iteration is directly dependent on point cloud

230 density, since high density point clouds will require higher a *knn* (Vicari et al., 2019). The utility package in

231 *TLSeparation* was used to automatically detect the optimum *knn* for each tree point cloud.

232 To voxelise individual tree complete (Figure 2a) and wood only (Figure 2b) point clouds, we used a modified

233 approach based on Lecigne et al. (2018), voxelising within the projected crown area of the whole tree point cloud

234 (Figure 2c) to calculate PAI. In the same way as for PAI, we calculated WAI using the separated wood point cloud

235 within the projected crown area of the whole tree (Figure 2d; using the whole crown and not just the wood point

236 cloud), and derived α for each tree as $WAI/_{PAI}$, allowing a comparison with existing literature estimating α for a

237 range of ecosystems, (Sea et al., 2011; Woodgate et al., 2016).

238 **2.6 Statistical Analyses**

239 We tested the relationships between PAI_{TLS} and PAI_{DHP} estimates using Standardised Major Axis (SMA) using

240 the open source *R* (R Core Team, 2020) package, *smatr* (Warton et al., 2012). SMA is an approach to estimating

241 a line of best fit where we are not able to predict one variable from another (Warton et al., 2006); we chose SMA

242 because we do not have a 'true' validation dataset, so avoid assuming either DHP or any of the TLS methods

243 produces the most accurate results. For each TLS method, we assessed the relationship with DHP using the

244 coefficient of determination and RMSE. We chose to compare PAI values rather than WAI or LAI as to do so

245 would mean an additional correction for non-photosynthetic elements, which each method does in different ways,

246 so introducing further source of uncertainty and limiting our ability to fairly compare processing approaches. To

247 further understand observed drivers of variance in PAI, we tested the relationship between PAI and whole plot

248 crown area index, CAI, a proxy measure of stand density and local competition (Caspersen et al., 2011; Coomes

249 et al., 2012). We calculated CAI as the sum of TLS-derived projected crown area, divided by the plot area (Owen

250 et al., 2021).

251

252 To test if α differs by species, we used linear mixed models (LMMs) in the *R* package, *lme4* (Bates et al., 2015).

253 We included an intercept only random plot effect to account for local effects on α:

254

255 $$\alpha_{i,sj} = \varphi_s + Plot_j, \tag{1}$$

256

257 here, α_i is α of an individual of species s, in plot j, and φ_s is the parameter to be fit. To test the effect of stand

258 structure and tree height on α, we fit relationships separately for each species, again including a random plot

259 effect:

260

261 $$\alpha_{i,sj} = \varphi_s + b_s\,H_i + c_s\,CAI_j + Plot_{sj.} \tag{2}$$

262

263 here H_i is the height of the tree, CAI_j is the crown area index for the plot, with other parameters as before.

264 For each species' model (equation 2), we calculated the intra-class correlation coefficient (ICC). The ICC, similar

265 to coefficient of determination, quantifies the amount of variance explained by the random effect in a linear mixed

266 model (Nakagawa et al., 2017).

267 **3. Results**

268 **3.1 Comparison of plant area index estimated by DHP and single scan TLS**

269 Of the two single scan TLS methods tested (*LiDAR Pulse* method and *2D Intensity Image* method), we found that

270 the relationship between PAI estimated using the *LiDAR Pulse* method and PAI$_{DHP}$, had a higher R^2 than the *2D*

271 *Intensity Image* method (SMA; *LiDAR Pulse* method $R^2 = 0.50$, slope $= 0.73$, $p < 0.001$, RMSE $= 0.14$, and *2D*

272 *Intensity Image* method $R^2 = 0.22$, slope $= 0.38$, $p < 0.001$, RMSE $= 0.39$, respectively, Figure 3a). At larger PAI

273 values, both TLS methods underestimated PAI relative to DHP (Figure 3b). We found statistically significant

274 negative correlations between residuals and DHP for both methods (SMA; *2D Intensity Image* method residuals

275 $R^2 = 0.85$, slope $= -0.88$, $p < 0.01$; *LiDAR Pulse* method residuals $R^2 = 0.47$, slope $= -0.70$, $p < 0.01$; Figure 3b).

276 The *2D Intensity Image* method showed larger underestimation at higher PAI$_{DHP}$ values, suggesting this method

277 may saturate sooner for higher PAI values than either DHP or the *LiDAR Pulse* method (Figure 3b).
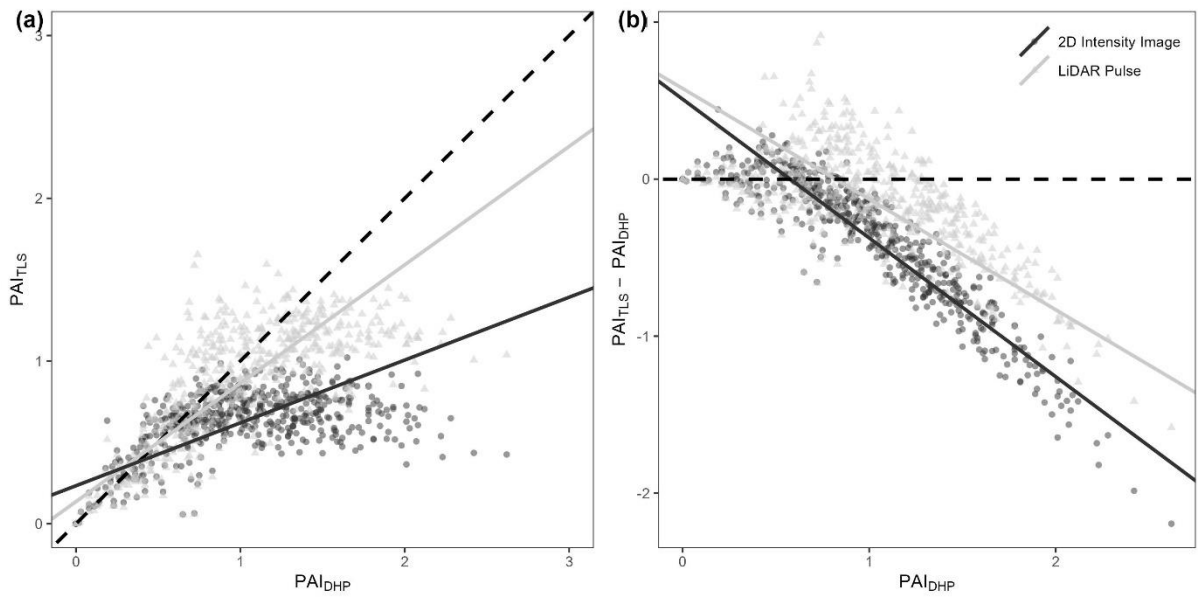
Figure 3: Comparison of single scan PAI$_{TLS}$ and PAI$_{DHP}$ estimates, for all 528 scan locations (16 per plot). (a) The correlation between DHP derived PAI with PAI derived using the 2D Intensity Image method R^2 = 0.22, slope = 0.38, p < 0.001, RMSE = 0.39 (circles), and LiDAR Pulse method R^2 = 0.50, slope = 0.73, p < 0.001, RMSE = 0.14 (triangles). Dashed line in panel (a) represents 1:1 relationship. (b) The difference between PAI$_{TLS}$ and PAI$_{DHP}$ estimates for the 2D Intensity Image method, and LiDAR Pulse method. Dashed line in panel (b) represents 0. Solid lines show statistically significant relationships fitted using SMA (p < 0.01).

3.2 Comparison of whole plot plant area index estimated using TLS and DHP and the effect of plot structure on PAI

We found statistically significant correlations between whole plot PAI$_{TLS}$ values and PAI$_{DHP}$ for all three TLS methods (Figure 4). As for single scans, the *LiDAR Pulse* method showed the closest agreement to PAI$_{DHP}$, here compared to both the *Voxel-Based* and *2D Intensity Image* methods (SMA; *LiDAR Pulse* method R^2 = 0.66, slope = 0.82, p < 0.01, RMSE = 0.14; *Voxel-Based* method R^2 = 0.39, slope = 2.76, p < 0.01, RMSE = 0.88; *2D Intensity Image* method R^2 = 0.35, slope = 0.36, p < 0.01, RMSE = 0.39, respectively; Figure 4a). The *2D Intensity Image* method and *LiDAR Pulse* method consistently underestimated PAI compared to DHP, whilst the *Voxel-Based* method underestimated in plots with lower PAI$_{DHP}$ and overestimated in plots with higher PAI$_{DHP}$. The *Voxel-Based* method's high PAI values compared to other methods is likely due to its use of multiple co-registered scans reducing occlusion effects prevalent in single scan data.

To assess the effect of plot structure on variation in TLS derived PAI, we compared PAI$_{TLS}$ estimates CAI (Figure 4b). We found a significant positive relationship between CAI and PAI estimated using each of the *LiDAR Pulse* method, the *Voxel-Based* method, and DHP (SMA*; LiDAR Pulse* method R^2 = 0.79, slope = 1.69, p < 0.01; *Voxel-Based* method R^2 = 0.76, slope = 5.72, p < 0.01; *2D Intensity Image* method R2 = 0.15, slope = 0.76, p < 0.05; DHP R^2 = 0.46, slope = 2.07, p < 0.01, respectively; Figure 4b), where the *2D Intensity Image* method shows signs of saturation at medium CAI values (Figure 4b).
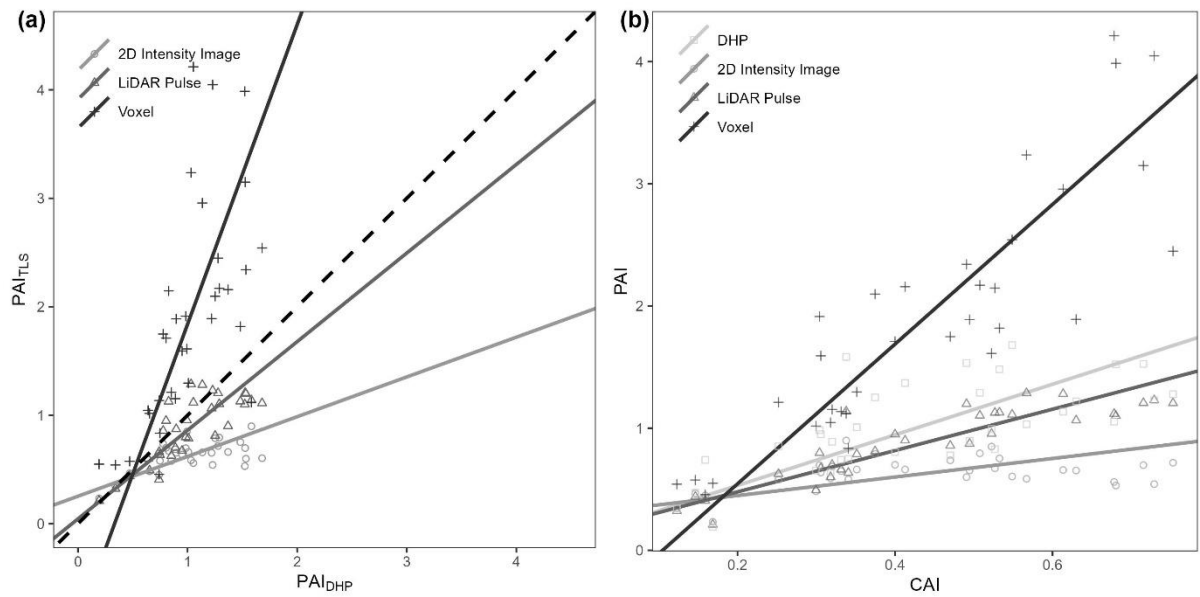
Figure 4: Comparison of plot level PAI$_{TLS}$ vs PAI$_{DHP}$, and CAI vs PAI estimates for all 33 plots. (a) The correlation between DHP derived PAI and PAI derived using 2D Intensity Image R^2 = 0.35, slope = 0.36, p < 0.01, RMSE = 0.39 (circle), LiDAR Pulse R^2 = 0.66, slope = 0.82, p < 0.01, RMSE = 0.14 (triangle) and Voxel-Based R^2 = 0.39, slope = 2.76, p < 0.01, RMSE = 0.88 (cross) methods (b) The correlation between TLS derived CAI and PAI derived using DHP R^2 = 0.46, slope = 2.07, p < 0.01 (square), 2D Intensity Image R^2 = 0.15, slope = 0.76, p < 0.05 (circle) LiDAR Pulse R^2 = 0.79, slope = 1.69, p < 0.01 (triangle) and Voxel-Based R^2 = 0.76, slope = 5.72, p < 0.01 (cross) methods. Lines show statistically significant relationships fitted using SMA (p < 0.01). Dashed line in panel (a) represents 1:1 relationship.

3.4 Influence of species, tree height and CAI on α

To understand drivers of variance in α, we used individual tree PAI and WAI, calculated using the *Voxel-Based* method to test the relationship between species and α, and height/ CAI and α. We found that more drought tolerant species generally had higher α values than less drought tolerant species (Table B1; Figure 5), however, confidence intervals were wide and overlapping, suggesting that species is not a strong predictor of variation in α. We found a statistically significant negative effect of height (p < 0.001; Table B2; Figure 6a) and positive effect of CAI (p < 0.01 – 0.05; Table B2; Figure 6b) on α for all species apart from *P. sylvestris*. α decreased more rapidly with height and increased less rapidly with CAI for oaks than pines. Statistically significant ICC values were higher for *P. nigra* (ICC = 0.211; Table B2) than *P. pinaster, Q. faginea* and *Q. ilex* (ICC = 0.036; 0.060; 0.070, respectively), showing that more α variation is explained by the random plot effect in *P. nigra* than the other species. *P. pinaster* has a wider confidence interval (Figure 5), possibly explained by its lower sample size. To understand drivers of variance in WAI we carried out additional analysis to test the relationship between WAI and species, height, CAI, and PAI, and presented these results in Appendix C (Figure C3; Tables C3, C4).
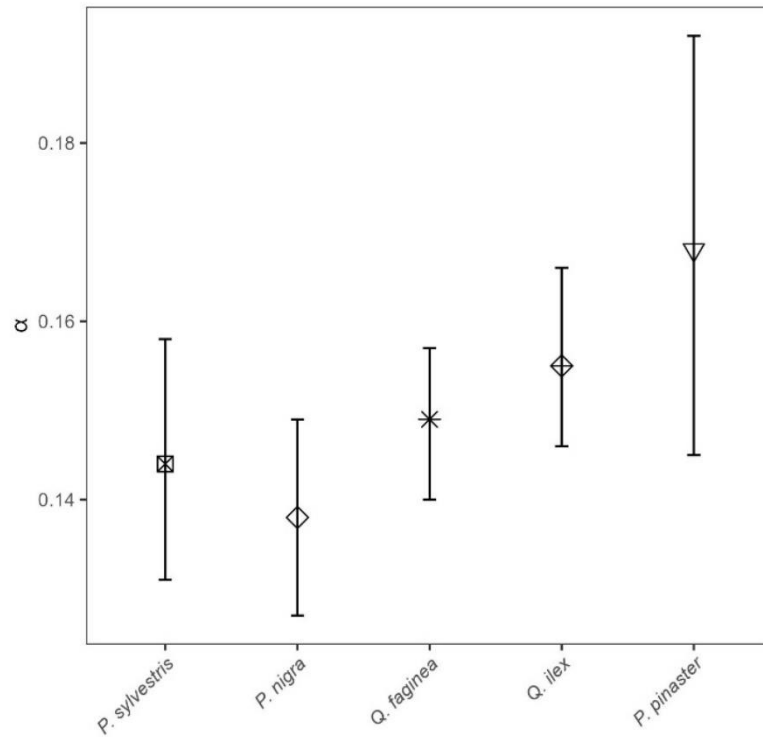
Figure 5: Linear mixed model derived α values (φ, equation 1) for all 2472 individual trees of species *P. sylvestris, P. nigra, Q. faginea, Q. ilex* and *P. pinaster*. Error bars represent 95% confidence intervals. Species are listed left to right from low – high drought tolerance, with the exception of *P. pinaster*, for which drought tolerance index has not been calculated in the literature. Drought tolerance rankings are taken from Niinemets and Valladares (2006).
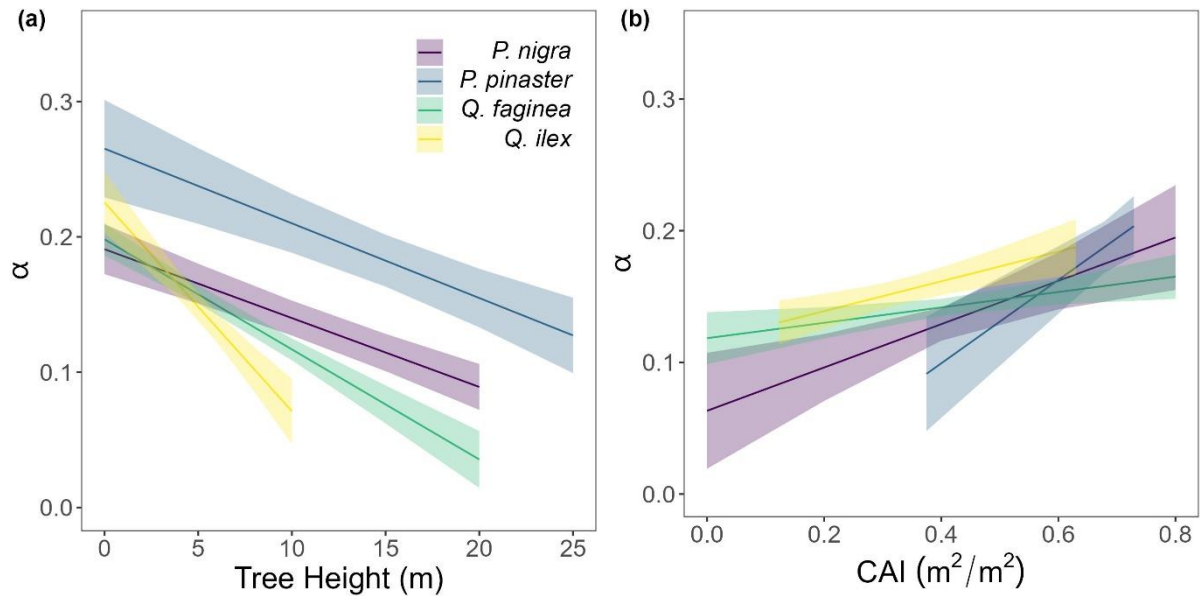

Figure 6: Variation in α for each species: *Pinus nigra, P. pinaster, Q. faginea* and *Q. ilex* with (a) height and (b) plot CAI. Lines represent statistically significant linear mixed models (equation 2; significance levels from p < 0.001 to p < 0.05). Ribbons represent 95% confidence intervals. The model for *P. sylvestris* was not statistically significant.

12

4. Discussion

4.1 Comparison of approaches to deriving PAI from remote sensed data

We found substantial differences in PAI values estimated from TLS and DHP and from different TLS processing methods (Figures 3 and 4). Further, differences between TLS methods varied across plot structure, with the greatest differences between methods in plots with high CAI, and therefore high canopy density. Although previous studies have presented TLS as an improvement over DHP due to its independence of illumination and sky conditions during the data acquisition phase, and ability to resolve fine-scale canopy elements and gaps (Calders et al., 2018; Grotti et al., 2020; Zhu et al., 2018), we have shown that there is large variability between TLS processing methods in Mediterranean forests. Rigorous intercomparison of approaches, ideally using standard benchmarking TLS datasets, and destructive sampling, would improve trust and reliability of TLS algorithms.

We found the *LiDAR Pulse* method (Jupp et al., 2008) to have the best agreement with DHP for both whole plot and single scan PAI estimates. In contrast to previous studies comparing PAI_{TLS} with PAI_{DHP} (Calders et al., 2018; Grotti et al., 2020; Woodgate et al., 2015), we found that the *LiDAR Pulse* and *2D Intensity Image* methods underestimated PAI compared to DHP, except at very low PAI values ($PAI_{TLS} < 0.5$). Quantification of PAI from DHP may introduce additional sources of error, for example, its relatively lower resolution compared to TLS could lead to mixed pixels that have a greater chance of misclassification of sky as vegetation (Jonckheere et al., 2004). This effect could be enhanced in a Mediterranean forest as trees in drier climates tend to have smaller leaves (Peppe et al., 2011), leading to more small canopy gaps that TLS may resolve where DHP cannot. Further, although we took steps to reduce the error introduced at DHP data acquisition and processing steps, including using automatic thresholding and collecting images with multiple exposures, DHP processing requires both model and user assumptions that can impact results. For example, PAI_{DHP} estimates are highly sensitive to camera exposure; increasing one stop of exposure can result in 3 – 28% difference in PAI and use of automatic exposure can result in up to 70% error (Zhang et al., 2005).

We found the *Voxel-Based* method overestimated PAI values compared to the other methods at the whole plot level. This is likely due to the method's use of co-registered scans, rather than averaged single scan PAI values, since co-registered scans will reduce occlusion effects prevalent in single scan data that could to lead to an underestimation of PAI (Wilkes et al., 2017). The *Voxel-Based* method is, however, sensitive to voxel size (Li et al., 2016), and larger voxels lead to larger PAI estimates as they are unable to capture all of the intricate details of canopy structure; we chose a voxel size of 0.05 m to match the minimum distance between points in our downsampled dataset. However, the *Voxel-Based* method is a memory intensive approach to calculating PAI, and smaller voxels have higher memory requirements. We picked this data resolution, and therefore voxel size, to balance the need to capture fine-scale canopy details against memory requirements for running the method on many large plot point clouds. Voxel size could have been chosen based on estimates' match to DHP, but this would assume (1) that DHP estimates are most accurate, and (2) that DHP data are always available, limiting the wider applicability of our findings. Understanding which method is over- or underestimating would require a destructively sampled dataset for validation, which was not possible for this study (or most ecosystems). However, other studies using voxel approaches have found that although these produce high LAI values for individual trees, these are underestimates compared with destructive samples (Li et al., 2016). Regardless, PAI and LAI estimates

using a *Voxel-Based* approach are highly dependent on voxel size (Li et al., 2016), and future work should test the influence of voxel size on PAI estimates, using destructive samples in a range of environments.

The relationship between the *LiDAR Pulse* method and TLS derived CAI had the highest R^2, demonstrating that the method is well suited to measuring PAI across the range of plot CAI values used in this study. Although the *2D Intensity Image* method can tackle the significant challenges presented by edge effects and partial beam interceptions, particularly present in phase-shift systems (Grotti et al., 2020), our results suggest this method has a lower performance ability, with saturation occurring sooner than all other methods in dense forests (Figures 3 and 4). The *2D Intensity Image* method uses the same raw single scan data as the *LiDAR Pulse* method, so the better performance from the latter is likely due to the method's use of vertically resolved gap fraction; both the *LiDAR Pulse* method and *Voxel-Based* method account for the vertical structure of the canopy by summing vertical slices through the canopy.

4.2 α variation between species and plot

We used the *Voxel-Based* method to investigate individual tree α variation between species and across structure, as this was the only approach we compared that could be applied to single tree point clouds which are leaf-wood separated. We found α values obtained were within the range of values obtained from destructive approaches (0.1 – 0.6, Gower et al., 1997). The drought and shade intolerant *P. nigra* showed stronger variability in α across plots (higher ICC value, Table B2) than other species, suggesting its wood – leaf ratio may be more sensitive to site factors. However, as the plots measured in this study vary in both abiotic conditions (altitude, aspect, slope, wetness) as well as species composition, stem density and canopy cover, there may be other drivers of variation in α values.

We found some evidence that species with higher drought tolerance had higher α values (Figure 5; Table B1), however, confidence intervals were wide, suggesting a weak relationship. There is evidence that trees that tolerate water limited environments have a lower leaf area (Battaglia et al., 1998; Mencuccini and Grace, 1995), so higher α values may reflect maintenance of homeostasis of leaf water use through adjustment of wood to leaf area ratio (Carter and White, 2009; Gazal et al., 2006). The potential for a tree to lose water is mostly regulated through leaf traits including stomatal conductance and leaf area, and both stand (Battaglia et al., 1998; Specht and Specht, 1989) and individual tree (Mencuccini, 2003) water use have been found to scale linearly with LAI, with drought often mitigated through leaf shedding (López et al., 2021).

4.3 Tree stature and stand density drives α variation

Although species had a weak relationship with α, tree height and plot CAI had a statistically significant relationship with α ($p < 0.001 – p < 0.05$) for all species, showing the importance of local stand structure on leaf and woody allocation. We found that α scaled negatively with height for all species apart from *P. sylvestris,* suggesting that in this environment, taller trees generally have a lower proportion of wood to plant area index than shorter ones. *P. sylvestris,* which is at the edge of its geographical range and physiological limits (Castro-Díez et al., 1997; Owen et al., 2021), showed no significant relationship between height and α. We found that α scaled positively with plot level CAI for all species apart from *P. sylvestris,* that is, trees growing in denser plots have a higher α. This supports theory that trees growing in dense forests are competing for resources, reducing individual tree leaf area (Jump et al., 2017). The negative relationships between height and α and positive relationships

410   between CAI and α relationships in our model suggest that trees may initially invest in vertical growth to reach
411   the canopy level, and once there invest in lateral growth, with more leaf area, to increase light capture. This
412   supports theory that trees grow to outcompete neighbouring individuals for light capture (Purves and Pacala, 2008)
413   and evidence that both lateral growth and LAI are reduced beneath closed canopies (Beaudet and Messier, 1998;
414   Canham, 1988).

415   Wood may be harder to accurately classify than leaves in TLS data (Vicari et al., 2019), resulting in a higher
416   occurrence of false positives in wood clouds, potentially leading to an overestimation in WAI, and therefore
417   underestimation of α, especially in trees with small leaves which are prevalent in dry, Mediterranean environments
418   (Peppe et al., 2011). The problem of misclassification will increase in taller trees due to TLS beam divergence,
419   occlusion and larger beam footprint at further distances (Vicari et al., 2019), suggesting that WAI overestimation
420   could be more pronounced in tall trees. Although our dense scanning strategy (Owen et al., 2021) was designed
421   to mitigate some of these effects, these effects mean our findings may underestimate the slope of the negative
422   relationship between α and tree height. Conversely, the increasing leaf-to-wood ratio could potentially be
423   explained by a greater number of empty voxels caused by occlusion in large trees. However, we took significant
424   steps to reduce occlusion, employing a 10 m scanning strategy that was developed in a dense tropical forest
425   (Wilkes et al., 2017).

4.4 Correcting for non-photosynthetic elements in LAI estimates using TLS

427   The value of TLS data to estimate individual tree PAI, WAI and subsequently α, demonstrates their potential to
428   corrective factors for non-photosynthetic components in ground based remote sensing measurements of LAI.
429   Properly correcting for WAI in LAI estimates is of global importance as small errors in ground based
430   measurements propagate through to large scale satellite observations generating large errors in global vegetation
431   models (Calders et al., 2018). The work presented here provides a foundation for future work combining multi-
432   source and multi-scale remote sensing datasets to correct largescale LAI products. Our results echo others' in
433   finding that the prevalence of woody material in the tree canopy, and therefore α, is dynamic and varies by species
434   as well as senescence, crown health and, in the case of deciduous forests, leaf phenology (Gower et al., 1999).
435   The use of single α value in a plot or region (Olivas et al., 2013; Woodgate et al., 2016), invariant of species, size
436   and forest structure, to convert PAI to LAI is therefore problematic (Niu et al., 2021). Our study demonstrates the
437   importance of taking species mix and structural variation into account when correcting for non-photosynthetic
438   material in ground-based LAI estimates.

5. Conclusions

440   We tested three methods for estimating PAI using Terrestrial Laser Scanning data and compared these against
441   traditional DHP measurements. We found large variation between PAI values estimated from each TLS method
442   and DHP, demonstrating that care should be taken when deriving PAI from ground based remote sensing methods.
443   Although the *LiDAR Pulse* method was found to have the best agreement with both single scan and whole plot
444   PAI values measured by DHP, the *Voxel-Based* method allowed separate analysis of the key metric used to correct
445   for the effect of WAI in LAI measurements, α, in individual trees. We recommend the *LiDAR Pulse* method as a
446   fast and effective method for PAI estimation independent of illumination conditions. Whilst the *Voxel-Based*
447   method may be used to analyse individual tree α and determine ecological drivers of variation, work remains to

448 determine the validity of these approaches, in particular correct voxel size choice. We found that α varies by
449 species, height and stand density, showing the importance of accurately correcting for WAI on the individual tree
450 level and the utility of TLS to do so.

451 The variation in our results for the different methods used to derive PAI from TLS data show that there is some
452 way to go before TLS derived vegetation indices can be interpreted as robust and reliable. Validation using
453 destructive samples and further intercomparison studies of methods are needed to demonstrate the advantages of
454 TLS, and use of benchmarking datasets should be standard. DHP is a faster, cheaper and more widely accessible
455 method for PAI estimation, and while TLS promises to alleviate potential bias in DHP estimates, results are highly
456 methods dependent. Our results demonstrate the challenges that stand in the way of large scale adoption of TLS
457 for vegetation indices monitoring.

458 **6. Code availability**

459 See https://github.com/will-flynn/tls_dhp_pai.git for all processing and modelling code.

460 **7. Data availability**

461 See Owen et al. (2022) for individual segmented tree data and Flynn et al. (2023) for thresholded DHP images.

462 **8. Author contribution**

463 All authors designed the study. HJFO and WRMF collected and processed TLS and DHP data; WRMF performed
464 formal analysis with guidance from all authors. WRMF led the writing with input from all authors. All authors
465 contributed critically to drafts and gave final approval for publication.

466 **9. Competing interests**

467 The authors declare that they have no conflict of interest.

468 **7. Acknowledgements**

471 **References**

472 Baeten, L., Verheyen, K., Wirth, C., Bruelheide, H., Bussotti, F., Finér, L., Jaroszewicz, B., Selvi, F.,
473 Valladares, F., Allan, E., Ampoorter, E., Auge, H., Avăcăriei, D., Barbaro, L., Bărnoaiea, I., Bastias, C. C.,
474 Bauhus, J., Beinhoff, C., Benavides, R., Benneter, A., Berger, S., Berthold, F., Boberg, J., Bonal, D.,
475 Brüggemann, W., Carnol, M., Castagneyrol, B., Charbonnier, Y., Chećko, E., Coomes, D., Coppi, A., Dalmaris,
476 E., Dănilă, G., Dawud, S. M., de Vries, W., De Wandeler, H., Deconchat, M., Domisch, T., Duduman, G.,
477 Fischer, M., Fotelli, M., Gessler, A., Gimeno, T. E., Granier, A., Grossiord, C., Guyot, V., Hantsch, L.,
478 Hättenschwiler, S., Hector, A., Hermy, M., Holland, V., Jactel, H., Joly, F.-X., Jucker, T., Kolb, S., Koricheva,
479 J., Lexer, M. J., Liebergesell, M., Milligan, H., Müller, S., Muys, B., Nguyen, D., Nichiforel, L., Pollastrini, M.,
480 Proulx, R., Rabasa, S., Radoglou, K., Ratcliffe, S., Raulund-Rasmussen, K., Seiferling, I., Stenlid, J., Vesterdal,
481 L., von Wilpert, K., Zavala, M. A., Zielinski, D., and Scherer-Lorenzen, M.: A novel comparative research
482 platform designed to determine the functional significance of tree species diversity in European forests,
483 Persepect. Plant. Ecol., 15, 281–291, https://doi.org/10.1016/j.ppees.2013.07.002, 2013.

484 Baret, F., Weiss, M., Lacaze, R., Camacho, F., Makhmara, H., Pacholcyzk, P., and Smets, B.: GEOV1: LAI and
485 FAPAR essential climate variables and FCOVER global time series capitalizing over existing products. Part1:
486 Principles of development and production, Remote Sens. Environ., 137, 299–309,
487 https://doi.org/10.1016/j.rse.2012.12.027, 2013.

488   Bates, D., Mächler, M., Bolker, B., and Walker, S.: Fitting Linear Mixed-Effects Models Using lme4, J. Sat.
489   Softw., 67, https://doi.org/10.18637/jss.v067.i01, 2015.

490   Battaglia, M., Cherry, M. L., Beadle, C. L., Sands, P. J., and Hingston, A.: Prediction of leaf area index in
491   eucalypt plantations: effects of water stress and temperature, Tree Physiol., 18, 521–528,
492   https://doi.org/10.1093/treephys/18.8-9.521, 1998.

493   Beaudet, M. and Messier, C.: Growth and morphological responses of yellow birch, sugar maple, and beech
494   seedlings growing under a natural light gradient, Can. J. Forest Res., 28, 1007–1015,
495   https://doi.org/10.1139/x98-077, 1998.

496   Béland, M., Baldocchi, D. D., Widlowski, J.-L., Fournier, R. A., and Verstraete, M. M.: On seeing the wood
497   from the leaves and the role of voxel size in determining leaf area distribution of forests with terrestrial LiDAR,
498   Agr. Forest Meterol., 184, 82–97, https://doi.org/10.1016/j.agrformet.2013.09.005, 2014.

499   Breda, N. J. J.: Ground-based measurements of leaf area index: a review of methods, instruments and current
500   controversies, J. Exp. Bot., 54, 2403–2417, https://doi.org/10.1093/jxb/erg263, 2003.

501   Burt, A., Disney, M., and Calders, K.: Extracting individual trees from lidar point clouds using treeseg, Methods
502   Ecol. Evol., 10, 438–445, https://doi.org/10.1111/2041-210X.13121, 2019.

503   Calders, K., Armston, J., Newnham, G., Herold, M., and Goodwin, N.: Implications of sensor configuration and
504   topography on vertical plant profiles derived from terrestrial LiDAR, Agr. Forest Meterol., 194, 104–117,
505   https://doi.org/10.1016/j.agrformet.2014.03.022, 2014.

506   Calders, K., Origo, N., Disney, M., Nightingale, J., Woodgate, W., Armston, J., and Lewis, P.: Variability and
507   bias in active and passive ground-based measurements of effective plant, wood and leaf area index, Agr. Forest
508   Meterol., 252, 231–240, https://doi.org/10.1016/j.agrformet.2018.01.029, 2018.

509   Calders, K., Adams, J., Armston, J., Bartholomeus, H., Bauwens, S., Bentley, L. P., Chave, J., Danson, F. M.,
510   Demol, M., Disney, M., Gaulton, R., Krishna Moorthy, S. M., Levick, S. R., Saarinen, N., Schaaf, C., Stovall,
511   A., Terryn, L., Wilkes, P., and Verbeeck, H.: Terrestrial laser scanning in forest ecology: Expanding the
512   horizon, Remote Sensing of Environment, 251, 112102, https://doi.org/10.1016/j.rse.2020.112102, 2020.

513   Canham, C. D.: Growth and Canopy Architecture of Shade-Tolerant Trees: Response to Canopy Gaps, Ecology,
514   69, 786–795, https://doi.org/10.2307/1941027, 1988.

515   Carter, J. L. and White, D. A.: Plasticity in the Huber value contributes to homeostasis in leaf water relations of
516   a mallee Eucalypt with variation to groundwater depth, Tree Physiol., 29, 1407–1418,
517   https://doi.org/10.1093/treephys/tpp076, 2009.

518   Caspersen, J. P., Vanderwel, M. C., Cole, W. G., and Purves, D. W.: How Stand Productivity Results from Size-
519   and Competition-Dependent Growth and Mortality, PLoS ONE, 6, e28660,
520   https://doi.org/10.1371/journal.pone.0028660, 2011.

521   Castro-Díez, P., Villar-Salvador, P., Pérez-Rontomé, C., Maestro-Martínez, M., and Montserrat-Martí, G.: Leaf
522   morphology and leaf chemical composition in three Quercus (Fagaceae) species along a rainfall gradient in NE
523   Spain, Trees, 11, 127–134, https://doi.org/10.1007/PL00009662, 1997.

524   Chen, J. M. and Black, T. A.: Defining leaf area index for non-flat leaves, Plant Cell Environ., 15, 421–429,
525   https://doi.org/10.1111/j.1365-3040.1992.tb00992.x, 1992.

526   Coomes, D. A., Holdaway, R. J., Kobe, R. K., Lines, E. R., and Allen, R. B.: A general integrative framework
527   for modelling woody biomass production and carbon sequestration rates in forests, Journal of Ecology, 100, 42–
528   64, https://doi.org/10.1111/j.1365-2745.2011.01920.x, 2012.

529   Disney, M.: Terrestrial LiDAR: a three-dimensional revolution in how we look at trees, New Phytol., 222,
530   1736–1741, https://doi.org/10.1111/nph.15517, 2018.

531 Flynn, W. R. M., Owen, H. J. F., Grieve, S. W. D., and Lines, E. R.: DHP images collected from Alto Tajo and
532 Cuellar in Spain. (V1), https://doi.org/10.5281/ZENODO.7628072, 2023.

533 Gazal, R. M., Scott, R. L., Goodrich, D. C., and Williams, D. G.: Controls on transpiration in a semiarid riparian
534 cottonwood forest, Agr. Forest Meterol., 137, 56–67, https://doi.org/10.1016/j.agrformet.2006.03.002, 2006.

535 Gower, S. T., Vogel, J. G., Norman, J. M., Kucharik, C. J., Steele, S. J., and Stow, T. K.: Carbon distribution
536 and aboveground net primary production in aspen, jack pine, and black spruce stands in Saskatchewan and
537 Manitoba, Canada, J. Geophys. Res., 102, 29029–29041, https://doi.org/10.1029/97JD02317, 1997.

538 Gower, S. T., Kucharik, C. J., and Norman, J. M.: Direct and Indirect Estimation of Leaf Area Index, fAPAR,
539 and Net Primary Production of Terrestrial Ecosystems, Remote Sens. Environ., 70, 29–51,
540 https://doi.org/10.1016/S0034-4257(99)00056-5, 1999.

541 Grotti, M., Calders, K., Origo, N., Puletti, N., Alivernini, A., Ferrara, C., and Chianucci, F.: An intensity, image-
542 based method to estimate gap fraction, canopy openness and effective leaf area index from phase-shift terrestrial
543 laser scanning, Agr. Forest Meterol., 280, 107766, https://doi.org/10.1016/j.agrformet.2019.107766, 2020.

544 Hardwick, S. R., Toumi, R., Pfeifer, M., Turner, E. C., Nilus, R., and Ewers, R. M.: The relationship between
545 leaf area index and microclimate in tropical forest and oil palm plantation: Forest disturbance drives changes in
546 microclimate, Agr. Forest Meterol., 201, 187–195, https://doi.org/10.1016/j.agrformet.2014.11.010, 2015.

547 Hijmans, R. J.: raster: Geographic Data Analysis and Modeling R package version 3.5-21, https://CRAN.R-
548 project.org/package=raster., 2022.

549 Hosoi, F. and Omasa, K.: Voxel-Based 3-D Modeling of Individual Trees for Estimating Leaf Area Density
550 Using High-Resolution Portable Scanning Lidar, IEE T. Geosci. Remote, 44, 3610–3618,
551 https://doi.org/10.1109/TGRS.2006.881743, 2006.

552 Itakura, K. and Hosoi, F.: Voxel-based leaf area estimation from three-dimensional plant images, J. Agric.
553 Meteorol., 75, 211–216, https://doi.org/10.2480/agrmet.d-19-00013, 2019.

554 Jonckheere, I., Fleck, S., Nackaerts, K., Muys, B., Coppin, P., Weiss, M., and Baret, F.: Review of methods for
555 in situ leaf area index determination, Agr. Forest Meterol., 121, 19–35,
556 https://doi.org/10.1016/j.agrformet.2003.08.027, 2004.

557 Jonckheere, I. G. C., Muys, B., and Coppin, P.: Allometry and evaluation of in situ optical LAI determination in
558 Scots pine: a case study in Belgium, Tree Physiol., 25, 723–732, https://doi.org/10.1093/treephys/25.6.723,
559 2005.

560 Jucker, T., Bouriaud, O., Avacaritei, D., Dănilă, I., Duduman, G., Valladares, F., and Coomes, D. A.:
561 Competition for light and water play contrasting roles in driving diversity-productivity relationships in Iberian
562 forests, J. Ecol., 102, 1202–1213, https://doi.org/10.1111/1365-2745.12276, 2014.

563 Jump, A. S., Ruiz-Benito, P., Greenwood, S., Allen, C. D., Kitzberger, T., Fensham, R., Martínez-Vilalta, J.,
564 and Lloret, F.: Structural overshoot of tree growth with climate variability and the global spectrum of drought-
565 induced forest dieback, Glob. Change Biol., 23, 3742–3757, https://doi.org/10.1111/gcb.13636, 2017.

566 Jupp, D. L. B., Culvenor, D. S., Lovell, J. L., Newnham, G. J., Strahler, A. H., and Woodcock, C. E.: Estimating
567 forest LAI profiles and structural parameters using a ground-based laser called 'Echidna(R), Tree Physiol., 29,
568 171–181, https://doi.org/10.1093/treephys/tpn022, 2008.

569 Kamoske, A. G., Dahlin, K. M., Stark, S. C., and Serbin, S. P.: Leaf area density from airborne LiDAR:
570 Comparing sensors and resolutions in a temperate broadleaf forest ecosystem, Forest Ecol. Manag., 433, 364–
571 375, https://doi.org/10.1016/j.foreco.2018.11.017, 2019.

572 Kuusk, V., Niinemets, Ü., and Valladares, F.: A major trade-off between structural and photosynthetic
573 investments operative across plant and needle ages in three Mediterranean pines, Tree Physiol., 38, 543–557,
574 https://doi.org/10.1093/treephys/tpx139, 2018.

Leblanc, S. G. and Chen, J. M.: A practical scheme for correcting multiple scattering effects on optical LAI measurements, Agr. Forest Meterol., 110, 125–139, https://doi.org/10.1016/S0168-1923(01)00284-2, 2001.

Lecigne, B., Delagrange, S., and Messier, C.: Exploring trees in three dimensions: VoxR, a novel voxel-based R package dedicated to analysing the complex arrangement of tree crowns, Ann. Bot-London, 121, 589–601, https://doi.org/10.1093/aob/mcx095, 2018.

Li, S., Dai, L., Wang, H., Wang, Y., He, Z., and Lin, S.: Estimating Leaf Area Density of Individual Trees Using the Point Cloud Segmentation of Terrestrial LiDAR Data and a Voxel-Based Model, Remote Sens-Basel, 9, 1202, https://doi.org/10.3390/rs9111202, 2017.

Li, Y., Guo, Q., Tao, S., Zheng, G., Zhao, K., Xue, B., and Su, Y.: Derivation, Validation, and Sensitivity Analysis of Terrestrial Laser Scanning-Based Leaf Area Index, Can. J. Remote Sens., 42, 719–729, https://doi.org/10.1080/07038992.2016.1220829, 2016.

Lines, E. R., Fischer, F. J., Owen, H. J. F., and Jucker, T.: The shape of trees: Reimagining forest ecology in three dimensions with remote sensing, J. Ecol., 110, 1730–1745, https://doi.org/10.1111/1365-2745.13944, 2022.

Long, J. N. and Smith, F. W.: Leaf area - sapwood area relations of lodgepole pine as influenced by stand density and site index., Can. J. Forest Res., 18, 247–250, 1988.

López, R., Cano, F. J., Martin-StPaul, N. K., Cochard, H., and Choat, B.: Coordination of stem and leaf traits define different strategies to regulate water loss and tolerance ranges to aridity, New Phytol., 230, 497–509, https://doi.org/10.1111/nph.17185, 2021.

Lovell, J. L., Jupp, D. L. B., van Gorsel, E., Jimenez-Berni, J., Hopkinson, C., and Chasmer, L.: Foliage Profiles from Ground Based Waveform and Discrete Point Lidar, SilviLaser, 1–9, 2011.

Ma, L., Zheng, G., Eitel, J. U. H., Magney, T. S., and Moskal, L. M.: Determining woody-to-total area ratio using terrestrial laser scanning (TLS), Agr. Forest Meterol., 228–229, 217–228, https://doi.org/10.1016/j.agrformet.2016.06.021, 2016.

Madrigal-González, J., Herrero, A., Ruiz-Benito, P., and Zavala, M. A.: Resilience to drought in a dry forest: Insights from demographic rates, Forest Ecol. Manag., 389, 167–175, https://doi.org/10.1016/j.foreco.2016.12.012, 2017.

Magnani, F., Mencuccini, M., and Grace, J.: Age-related decline in stand productivity: the role of structural acclimation under hydraulic constraints, Plant Cell Environ., 23, 251–263, https://doi.org/10.1046/j.1365-3040.2000.00537.x, 2000.

Mencuccini, M.: The ecological significance of long-distance water transport: short-term regulation, long-term acclimation and the hydraulic costs of stature across plant life forms, Plant Cell Environ., 26, 163–182, https://doi.org/10.1046/j.1365-3040.2003.00991.x, 2003.

Mencuccini, M. and Grace, J.: Climate influences the leaf area/sapwood area ratio in Scots pine, Tree Physiol., 15, 1–10, https://doi.org/10.1093/treephys/15.1.1, 1995.

Monsi, M. and Saeki, T.: On the Factor Light in Plant Communities and its Importance for Matter Production, Ann. Bot-London, 95, 549–567, https://doi.org/10.1093/aob/mci052, 1953.

Nakagawa, S., Johnson, P. C. D., and Schielzeth, H.: The coefficient of determination R2 and intra-class correlation coefficient from generalized linear mixed-effects models revisited and expanded, J. R. Soc. Interface, 14, 20170213, https://doi.org/10.1098/rsif.2017.0213, 2017.

Niinemets, Ü. and Valladares, F.: Tolerance to shade, drought, and waterlogging of temperate northern hemisphere trees and shrubs, Ecol. Monogr., 76, 521–547, https://doi.org/10.1890/0012-9615(2006)076[0521:TTSDAW]2.0.CO;2, 2006.

618 Niu, X., Fan, J., Luo, R., Fu, W., Yuan, H., and Du, M.: Continuous estimation of leaf area index and the
619 woody-to-total area ratio of two deciduous shrub canopies using fisheye webcams in a semiarid loessial region
620 of China, Ecol. Indic., 125, 107549, https://doi.org/10.1016/j.ecolind.2021.107549, 2021.

621 Olivas, P. C., Oberbauer, S. F., Clark, D. B., Clark, D. A., Ryan, M. G., O'Brien, J. J., and Ordoñez, H.:
622 Comparison of direct and indirect methods for assessing leaf area index across a tropical rain forest landscape,
623 Agr. Forest Meterol., 177, 110–116, https://doi.org/10.1016/j.agrformet.2013.04.010, 2013.

624 Owen, H. J. F., Flynn, W. R. M., and Lines, E. R.: Competitive drivers of inter-specific deviations of crown
625 morphology from theoretical predictions measured with Terrestrial Laser Scanning, J. Ecol., 109, 2612–2628,
626 https://doi.org/10.1111/1365-2745.13670, 2021.

627 Owen, H. J. F., Flynn, W. R. M., and Lines, E. R.: Individual TLS tree clouds collected from both Alto Tajo and
628 Cuellar in Spain., 2022.

629 Peppe, D. J., Royer, D. L., Cariglino, B., Oliver, S. Y., Newman, S., Leight, E., Enikolopov, G., Fernandez-
630 Burgos, M., Herrera, F., Adams, J. M., Correa, E., Currano, E. D., Erickson, J. M., Hinojosa, L. F., Hoganson, J.
631 W., Iglesias, A., Jaramillo, C. A., Johnson, K. R., Jordan, G. J., Kraft, N. J. B., Lovelock, E. C., Lusk, C. H.,
632 Niinemets, Ü., Peñuelas, J., Rapson, G., Wing, S. L., and Wright, I. J.: Sensitivity of leaf size and shape to
633 climate: global patterns and paleoclimatic applications, New Phytol., 190, 724–739,
634 https://doi.org/10.1111/j.1469-8137.2010.03615.x, 2011.

635 Pfeifer, M., Gonsamo, A., Disney, M., Pellikka, P., and Marchant, R.: Leaf area index for biomes of the Eastern
636 Arc Mountains: Landsat and SPOT observations along precipitation and altitude gradients, Remote Sens.
637 Environ., 118, 103–115, https://doi.org/10.1016/j.rse.2011.11.009, 2012.

638 Phillips, N., Bond, B. J., McDowell, N. G., Ryan, M. G., and Schauer, A.: Leaf area compounds height-related
639 hydraulic costs of water transport in Oregon White Oak trees, Funct. Ecol., 17, 832–840,
640 https://doi.org/10.1111/j.1365-2435.2003.00791.x, 2003.

641 Purves, D. and Pacala, S.: Predictive Models of Forest Dynamics, Science, 320, 1452–1453,
642 https://doi.org/10.1126/science.1155359, 2008.

643 Ridler, T. W. and Calvard, S.: Picture Thresholding Using an Iterative Selection Method, IEEE T. Syst. Man.
644 Cyb., 8, 630–632, https://doi.org/10.1109/TSMC.1978.4310039, 1978.

645 Sea, W. B., Choler, P., Beringer, J., Weinmann, R. A., Hutley, L. B., and Leuning, R.: Documenting
646 improvement in leaf area index estimates from MODIS using hemispherical photos for Australian savannas,
647 Agr. Forest Meterol., 151, 1453–1461, https://doi.org/10.1016/j.agrformet.2010.12.006, 2011.

648 Specht, R. L. and Specht, A.: Canopy structure in Eucalyptus-dominated communities in Australia along
649 climatic gradients, Canopy structure in Eucalyptus-dominated communities in Australia along climatic
650 gradients, 10, 191–213, 1989.

651 Vicari, M. B., Disney, M., Wilkes, P., Burt, A., Calders, K., and Woodgate, W.: Leaf and wood classification
652 framework for terrestrial LiDAR point clouds, Methods Ecol. Evol., 10, 680–694, https://doi.org/10.1111/2041-
653 210X.13144, 2019.

654 Warton, D. I., Wright, I. J., Falster, D. S., and Westoby, M.: Bivariate line-fitting methods for allometry, Biol.
655 Rev., 81, 259–291, https://doi.org/10.1017/S1464793106007007, 2006.

656 Warton, D. I., Duursma, R. A., Falster, D. S., and Taskinen, S.: smatr 3 - an R package for estimation and
657 inference about allometric lines: *The smatr 3 - an R package*, Methods Ecol. Evol., 3, 257–259,
658 https://doi.org/10.1111/j.2041-210X.2011.00153.x, 2012.

659 Weiss, M., Baret, F., Smith, G. J., Jonckheere, I., and Coppin, P.: Review of methods for in situ leaf area index
660 (LAI) determination, Agr. Forest Meterol., 121, 37–53, https://doi.org/10.1016/j.agrformet.2003.08.001, 2004.

661 Whitehead, D.: The Estimation of Foliage Area from Sapwood Basal Area in Scots Pine, Forestry, 51, 137–149,
662 https://doi.org/10.1093/forestry/51.2.137, 1978.

663   Wilkes, P., Lau, A., Disney, M., Calders, K., Burt, A., Gonzalez de Tanago, J., Bartholomeus, H., Brede, B., and
664   Herold, M.: Data acquisition considerations for Terrestrial Laser Scanning of forest plots, Remote Sensing of
665   Environment, 196, 140–153, https://doi.org/10.1016/j.rse.2017.04.030, 2017.

666   Woodgate, W., Jones, S. D., Suarez, L., Hill, M. J., Armston, J. D., Wilkes, P., Soto-Berelov, M., Haywood, A.,
667   and Mellor, A.: Understanding the variability in ground-based methods for retrieving canopy openness, gap
668   fraction, and leaf area index in diverse forest systems, Agr. Forest Meterol., 205, 83–95,
669   https://doi.org/10.1016/j.agrformet.2015.02.012, 2015.

670   Woodgate, W., Armston, J. D., Disney, M., Jones, S. D., Suarez, L., Hill, M. J., Wilkes, P., and Soto-Berelov,
671   M.: Quantifying the impact of woody material on leaf area index estimation from hemispherical photography
672   using 3D canopy simulations, Agr. Forest Meterol., 226–227, 1–12,
673   https://doi.org/10.1016/j.agrformet.2016.05.009, 2016.

674   Zhang, Y., Chen, J. M., and Miller, J. R.: Determining digital hemispherical photograph exposure for leaf area
675   index estimation, Agr. Forest Meterol., 133, 166–181, https://doi.org/10.1016/j.agrformet.2005.09.009, 2005.

676   Zheng, G., Moskal, L. M., and Kim, S.-H.: Retrieval of Effective Leaf Area Index in Heterogeneous Forests
677   With Terrestrial Laser Scanning, IEEE T. Geosci. Remote, 51, 777–786,
678   https://doi.org/10.1109/TGRS.2012.2205003, 2013.

679   Zhu, X., Skidmore, A. K., Wang, T., Liu, J., Darvishzadeh, R., Shi, Y., Premier, J., and Heurich, M.: Improving
680   leaf area index (LAI) estimation by correcting for clumping and woody effects using terrestrial laser scanning,
681   Agr. Forest Meterol., 263, 276–286, https://doi.org/10.1016/j.agrformet.2018.08.026, 2018.

682